Chapter 5

The Fundamental Plane

5.1 Introduction

The $D_n - \sigma$ and FP relations have been obtained in the past using photometric measurements in many different bands, from B (Faber *et al.* 1989) to V (Lucey *et al.* 1991a,b) , r_G (Djorgovski & Davis 1987), Gunn r (Jørgensen, Franx & Kjærgaard 1996), and Cron-Cousins R (Colless *et al.* 1993). In the study of early-type galaxies there are no compelling reasons for favoring one optical band over the others, because early-type galaxies are almost dust-free and therefore extinction is not important in this case. Our adoption of I band for photometry was mainly dictated by the practical notion that cluster images contain several galaxies per frame, both of early– and late–type, and thus can be useful for TF application, where the I band is favored for compatibility with G97a,b.

Clusters of galaxies have been favorite targets for FP studies because they provide both an environment rich in early-type galaxies and large samples of objects all roughly at the same distance. Recent studies of that nature include those of Guzmán *et al.* (1993), Jørgensen *et al.* (1996) and that of the so called E-far collaboration (Wegner *et al.* 1996, and references therein). There is remarkable quantitative agreement in the FP calibration of the first two studies, while no result regarding the calibration of the FP relation has been published yet by the E-far collaboration.

Here the choice of clusters has fallen on some of the best studied ones in the sample of G97a,b, in order to make possible a comparison of the most accurate TF and FP peculiar velocity estimates. Clusters were selected only in the northern hemisphere, to facilitate spectroscopic observations with the 5m telescope of the Palomar Observatory. The clusters were also chosen to cover a large span of dynamical and intra-cluster medium properties, to facilitate the possible detection of environment-related differences in the FP relation among different clusters.

5.2 Fitting algorithms

The choice of an algorithm to find the "best" fit that describes the correlation between two or three variables is a non-trivial exercise. Whenever a significant amount of dispersion is present in the data (which can be either intrinsic, or due to measurement errors, or to a combination of the two), different algorithms produce different results.

Also, and this is what is most important, different algorithms respond differently to the biases that affect the data-set one is trying to fit. Another important point is that the most commonly used linear regression algorithms are based on the assumption that the independent variables are measured with infinite accuracy, and only the dependent variable has an uncertainty associated with it, which is not the case with real data. Further complications arise from the fact that the algorithms that correctly take into account errors in all the variables involved consider those errors as statistically independent, and this is not the case with the TF and FP relations.

Currently the best approach takes into account errors in all variables and uses Monte Carlo simulations that reproduce as closely as possible the biases present in the data-set being fitted. In this way it is possible to measure quantitatively the effects that those biases have on the final "best fit" relation, and compensate the results appropriately (see G97b).

For a linear relation with just two variables (like the TF relation) a ready-to-use maximum likelihood algorithm that takes into account errors in both variables is given by Press *et al.* (1992). The generalization to the three variables case, with errors in all three variables, is trivial. The Press *et al.* *fitexy* algorithm minimizes a chi-square merit function which is given by the weighted sum of the squares of the orthogonal distances of individual data-points from the fitting straight line. The weights are given by the total uncertainties associated with those distances, derived adding together the uncertainties in the two separate variables being correlated. The orthogonal distance d of a point $(x_\circ, y_\circ)$ from a straight line $y = a + bx$ is given by

$$d^2 = \frac{(a + bx_\circ - y_\circ)^2}{1 + b^2}$$

If the point is determined with uncertainties (ϵ_x, ϵ_y), then the uncertainty on the distance d is given by

$$\epsilon_d^2 = \frac{\epsilon_y^2 + b^2\epsilon_x^2}{1 + b^2} \tag{5.1}$$

Therefore the sum of the squares of the weighted distances of a set of points from a line is

$$\chi^2(a, b) = \sum_i \frac{d_i^2}{\epsilon_{d_i}^2} = \sum_i \frac{(a + bx_i - y_i)^2}{\epsilon_{y_i}^2 + b^2\epsilon_{x_i}^2} \tag{5.2}$$

which is Press *et al.*'s equation (15.3.2). Similarly the square of the orthogonal distance d of a point $(x_\circ, y_\circ, z_\circ)$ from a plane $z = a + bx + cy$ is given by

$$d^2 = \frac{(a + bx_\circ + cy_\circ - z_\circ)^2}{1 + b^2 + c^2} \tag{5.3}$$

and its relative uncertainty, when the point is determined with uncertainties $(\epsilon_x, \epsilon_y, \epsilon_z)$, is given by

$$\epsilon_d^2 = \frac{\epsilon_z^2 + b^2\epsilon_x^2 + c^2\epsilon_y^2}{1 + b^2 + c^2} \tag{5.4}$$

Therefore the sum of the squares of the weighted distances becomes

$$\chi^2(a, b, c) = \sum_i \frac{(a + bx_i + cy_i - z_i)^2}{\epsilon_{z_i}^2 + b^2\epsilon_{x_i}^2 + c^2\epsilon_{y_i}^2} \tag{5.5}$$

This weighted orthogonal fit will be used in the remainder of this chapter to fit the FP relation.

However, a modification to equation (5.5) is required by the fact that the errors in $\log R_e$ and μ_e in the FP are highly correlated (see section 3.6). From the general expression that gives the propagation of errors in case of non-zero covariance between variables, we write the error on the distance as

$$\epsilon_d^2 = \frac{\epsilon_z^2 + b^2\epsilon_x^2 + c^2\epsilon_y^2 - 2c\epsilon_z\epsilon_y R}{1 + b^2 + c^2} \tag{5.6}$$

where R is the linear correlation coefficient (also known as the Pearson correlation coefficient) between the two correlated quantities, assumed here to be y and z. Therefore the FP relation is found by minimizing the chi-square function

$$\chi^2(a,b,c) = \sum_i \frac{(a + b\log\sigma_v + c\mu_e - \log R_e)^2}{\epsilon_{\log R_e}^2 + b^2\epsilon_{\log\sigma_v}^2 + c^2\epsilon_{\mu_e}^2 - 2c\epsilon_{\log R_e}\epsilon_{\mu_e}R_{(\log R_e - \mu_e)}} \tag{5.7}$$

with respect to the three parameters a, b, and c.

5.3 Incompleteness bias

Galaxy samples are generally selected on the basis of the apparent galaxy optical luminosity. Bright galaxies are easier to spot on the photographic plates from which the most commonly used catalogs of galaxies, like the Catalog of Galaxies and Clusters of Galaxies (CGCG, Zwicky *et al.* 1968) and the Uppsala General Catalog (UGC, Nilson 1973), were produced. However, a selection based on the apparent magnitude (or angular size) introduces biases in a sample. The most important one is generally called the Malmquist bias: because galaxies (or stars, for that matter) do not have all the same luminosity, intrinsically faint and distant ones are systematically missing from the sample, whereas both intrinsically bright and faint ones can be seen among the nearby objects. Therefore the mean luminosity of the objects included in a flux-limited sample changes with distance, even if the true mean luminosity of the entire population does not. To avoid this bias one would need a catalog selected on the basis of the luminosity of the objects. Such a sample is usually called a volume-limited sample. Relations such as the TF and the FP are affected by the Malmquist bias, when they are applied to magnitude-limited samples. Because of the scatter present in those relations, galaxies of a given rotation velocity (for the TF), or with a given combination of velocity dispersion and surface brightness (for the FP), do not all have the same magnitude (TF) or effective radius (FP). Therefore the systematic lack of faint distant objects biases the observed relation with respect to the "true" one that would describe a volume-limited sample.

Cluster samples are composed of galaxies all at the same distance, and therefore they are not affected by the traditional Malmquist bias. However, because the scatter in the TF and FP relations is much smaller than the total range of magnitudes covered by both elliptical and spiral galaxies, a bias very similar to the Malmquist bias affects the application of those two relations to magnitude-limited cluster samples. Consider the TF relation, for example. For a given rotation velocity close to the bright end of the relation, all the galaxies within the relation's dispersion are bright enough to be included in the sample. For a rotation velocity close to the faint end of the relation, instead, only the brightest objects within the relation dispersion are included in the sample. This kind of bias is generally referred to as the cluster population incompleteness bias (Teerikorpi 1987, Sandage 1994a,b).

A number of recipes have been derived to correct the distances derived using the TF and FP relations for the effects of the Malmquist and population incompleteness bias (see Sandage 1994a, and references therein). However these analytical formulations all assume a rigorously magnitude-limited sample, which is almost never the case for real data-sets. The low accuracy of the catalog magnitudes used for the original sample selection, and various observational constraints result in final samples that have a gradually decreasing degree of completeness, instead of a sharply defined limit. Also, these analytical solutions assume that the errors and the scatter in the relations are uniform and constant for all values of the parameters involved, and again this is not the case in real samples. Rotation velocities and velocity dispersions, for example, are measured with an uncertainty that is almost independent of the galaxy magnitude, and therefore the fractional accuracy of those measurements changes significantly from one end of the relation to the other one.

A more accurate quantification of the bias effects on distance measurements can be obtained using Monte Carlo simulations to reproduce as accurately as possible the sample selection and error distribution characteristics. This approach was first used by G97b. The simulations also allow one to quantify the possible amplification of sample biases introduced by the particular fitting technique being employed. In the case of the FP relation, Monte Carlo simulations are even more important because the sample incompleteness affects the relation only indirectly, through the existing correlations between luminosity and effective radius (Fish 1964), velocity dispersion (Faber & Jackson 1976), and effective surface brightness (Binggeli, Sandage & Tarenghi 1984). These $L - R_e$, $L - \sigma$, and $L - \mu_e$ relations all show rather large scatter. Therefore, at any given velocity dispersion or effective surface brightness, the systematic lack of fainter galaxies is only marginally reflected into a lack of small effective radius objects, and it is not possible to translate the completeness of a sample directly into an effective radius, velocity dispersion or effective surface brightness completeness.

Our simulations are therefore designed to reproduce as closely as possible the observed relations between R_e and σ and the galaxy luminosity, and the relation between R_e and μ_e (Kormendy 1977). Then we select galaxies according to their magnitude, reproducing the observed luminosity incompleteness, and measure the indirect effect of this incompleteness on the FP parameters. The completeness is computed comparing the distribution of magnitudes in the FP sample with the one expected on the basis of the luminosity function (LF) of E and S0 galaxies. This is known to have an approximately Gaussian shape, when only giant galaxies are considered (Sandage, Binggeli & Tammann 1985). The histograms in Figure 5.1 show the magnitude distributions for the galaxies in our photometric sample. The shaded portion of the histogram gives the fraction of objects that are included in the FP sample. The solid curve is the best fitting Gaussian to the magnitude distribution of the photometric sample. The ratio of the number of objects in the FP sample to the number predicted in the same bin by the fitted Gaussian distribution gives the completeness for that particular magnitude bin. At the bright end of the distribution, where there are only 1-2 galaxies per bin the completeness has been arbitrarily normalized to one, based on the observation that in all clusters the brightest galaxies are always included in the FP sample. The histograms of

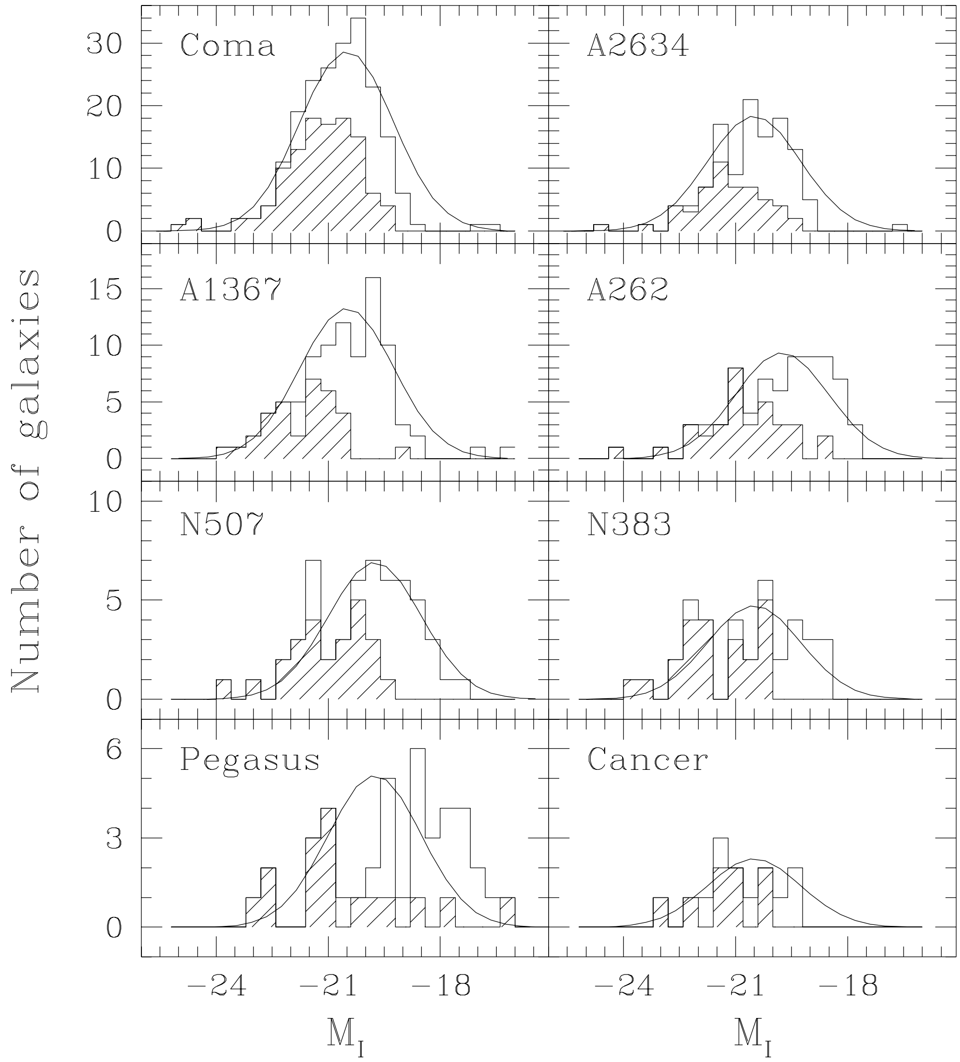

Figure 5.1 Absolute magnitude distribution for the galaxies in our photometric samples. All histograms have bins of 0.4 magnitudes. The shaded portion of each histogram identifies the fraction of the objects that are included in the FP sample. The solid line is the best fitting Gaussian luminosity function for the entire photometric sample.

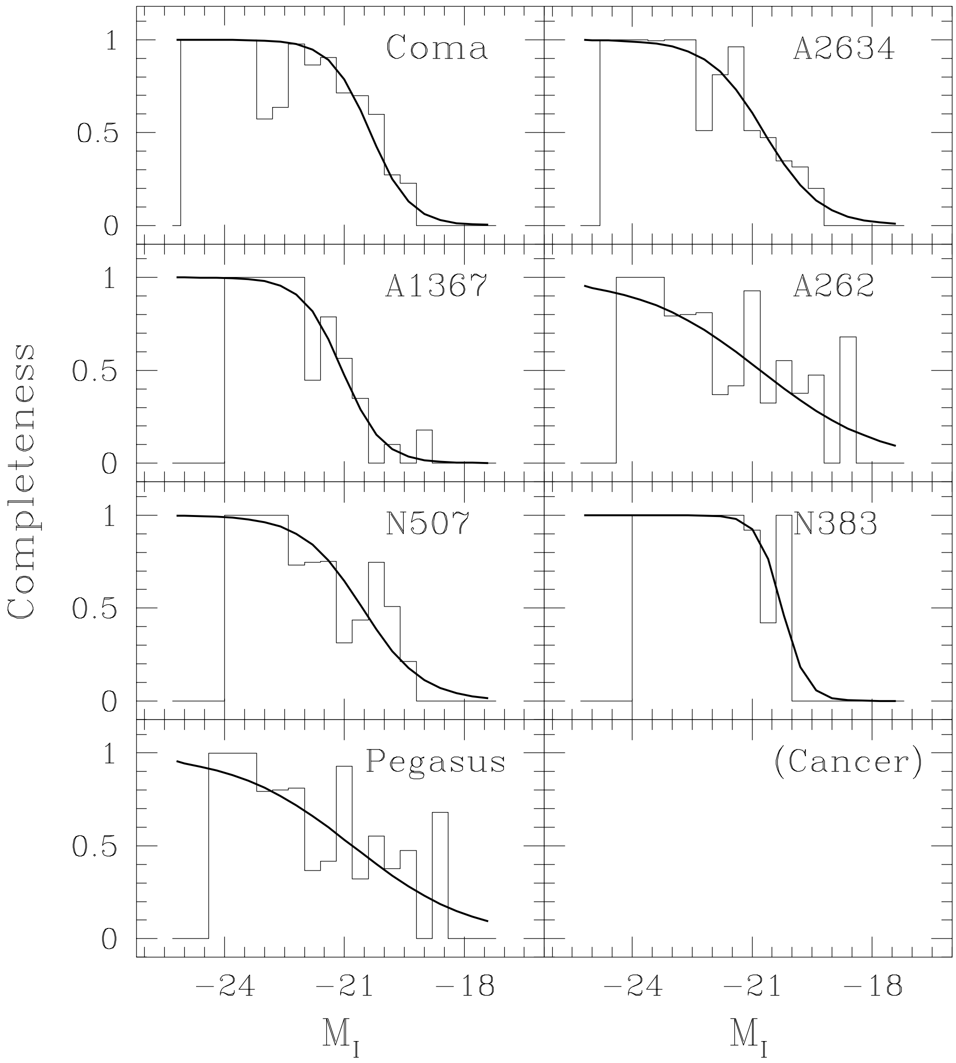

Figure 5.2 Completeness of the FP samples. The histograms represent the ratio of the number of objects included in the FP sample to the number predicted by the Gaussian luminosity function of Figure 5.1. The solid line is the best fitting Fermi-Dirac distribution to the completeness histogram. No completeness is computed for Cancer, because the photometric and spectroscopic samples are too small.

Table 5.1 FP sample completeness

Cluster	$M_{0.5}$ (E_F)	width (kT)
N383 gr.	-20.25	0.10
N507 gr.	-20.55	0.75
A262	-20.80	1.50
Cancer[a]	-20.15	0.65
A1367	-21.05	0.50
Coma	-20.35	0.50
Pegasus	-20.15	0.65
A2634	-20.70	0.70

[a] Completness parameters for Cancer assumed to be equal to those of Pegasus, and not computed from the photometric and spectroscopic sample (they are both too small).

Figure 5.2 show the completeness distribution for the various cluster samples. Following the approach of G97b, this has been fitted with a Fermi-Dirac distribution, which is shown in each panel by the solid line. The fitted Fermi-Dirac distributions are then used in the Monte Carlo simulations to reproduce the completeness of the real samples. Their parameters are listed in Table 5.1. The uncertainty on the half-completeness magnitude $M_{0.5}$ are approximately 0.2 magnitudes. In the case of the Cancer cluster, both the photometric and the spectroscopic samples are too small for a reliable fit. Given the similarity of this sample to that of the Pegasus cluster one, we use for Cancer the same completeness function derived for Pegasus.

The bias correction is computed for each cluster sample using the following procedure: first a mean complete sample and a mean incomplete one are obtained from a large number of Monte Carlo realizations of a sample that matches, in the incomplete realization, the characteristics of the particular real sample under exam; these two mean samples are then binned according to the value of the parameter $\log\sigma + 0.21(\mu_e - 19.45)$, which is the combination of $\log\sigma$ and μ_e that provides an edge-on view of the fundamental plane; finally the mean value of $\log R_e$ for each bin is measured, and the distributions of mean values obtained for the complete and incomplete sample are compared. Because of the lack of low luminosity objects, the mean $\log R_e$ measured in the incomplete sample is systematically larger than the one measured for the complete sample, except in the two to three bins which include the most luminous galaxies. These differences are fitted with a low order polynomial, and this is used to derive a correction to the observed value of $\log R_e$ of each galaxy. Thus the data-set obtained using the corrected values of $\log R_e$ should reproduce a sample which is statistically as close as possible to an unbiased one. The panels of Figure 5.3 show the bias corrections for the clusters in our sample: the points are the mean differences in $\log R_e$ measured in the simulations, and the solid line is the fitted polynomial that is used to compute the corrections. The mean correction to $\log R_e$ is approximately –0.012, although the actual correction depends quite strongly on the position of the galaxy in the FP diagram.

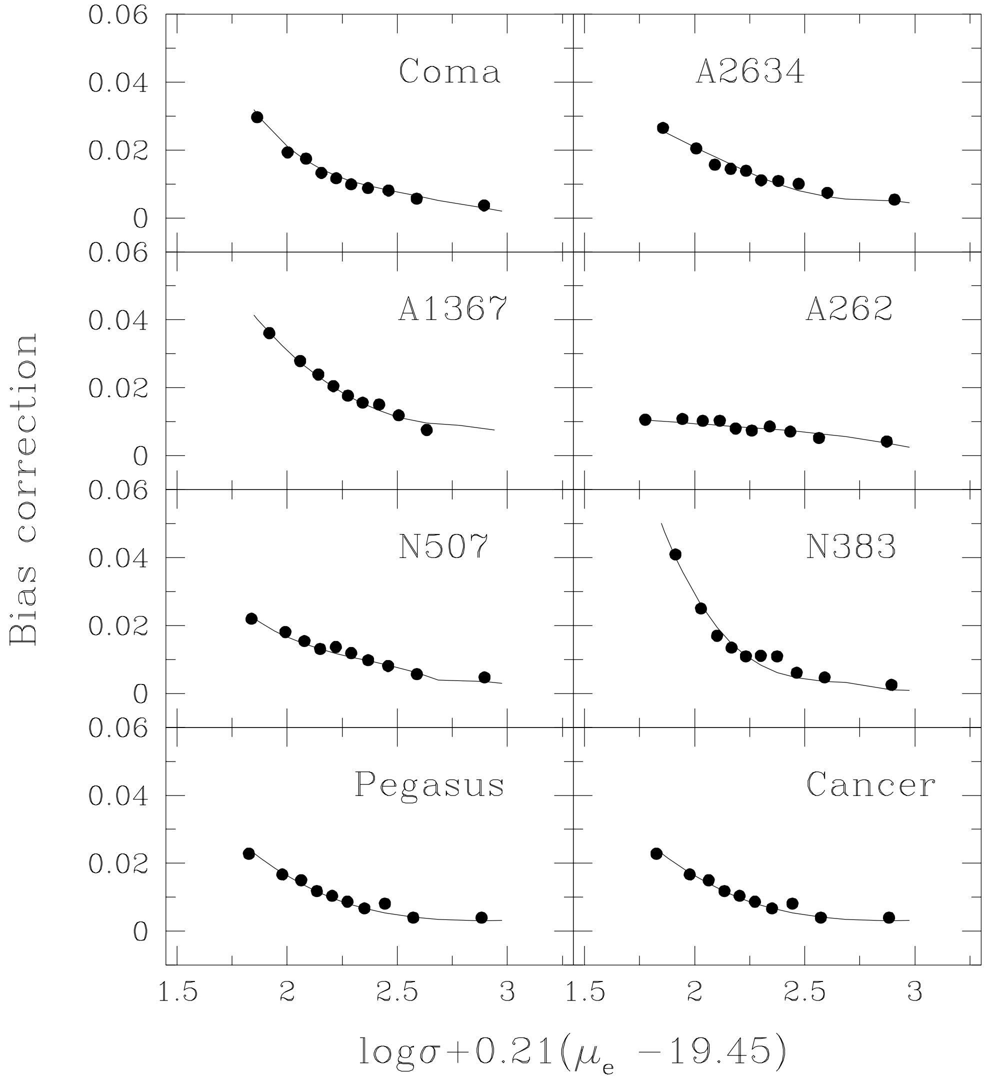

Figure 5.3 Bias corrections. The points represent the mean bias in $\log R_e$ derived from the simulations, and the solid line is the best fitting third order polynomial to these points. For Cancer the corrections computed for the Pegasus sample are used.

5.4 The Fundamental Plane in the I band

The I band FP template has been obtained combining six individual cluster samples (NGC 507, A262, A1367, Coma, Pegasus, A2634), under the assumption that, on average, these clusters are at rest with respect to the CMB reference frame. The Cancer cluster was excluded because of the uncertain completeness correction. The NGC 383 group was excluded because it is too close to the NGC 507 group, and most likely the two groups have similar peculiar velocities (see section 5.5). The presence of two correlated data-sets in a sample composed only of seven clusters would give very high weight to the NGC 383 - NGC 507 groups in determining the average FP reference frame. To avoid this, we prefer to determine the FP template using only six clusters, and a slightly smaller total number of objects (266 galaxies instead of 294). The derivation of the $\log R_e$, $\log \sigma$ and μ_e parameters for all galaxies in this sample has been discussed in Chapter 3 (photometric parameters), and Chapter 4 (spectroscopic parameters). Table A.5 in the appendix summarizes all these parameters for the global eight cluster sample.

To obtain the FP template a chi-square fitting algorithm, as in Section 5.2, has been used, in an iterative procedure: at each iteration the different samples have been combined using fixed values for the $\log \sigma$ and μ_e coefficients in the FP, and leaving as free variables the individual cluster peculiar velocities, which translate into systematic shifts in the value of $\log R_e$ for all cluster members, according to the relation

$$\frac{\Delta v}{v} = dex(\Delta \log R_e) - 1 \tag{5.8}$$

where Δv is the cluster peculiar velocity, and $v = cz$ is its redshift. When the minimum chi-square for the combination is found, the whole sample is fitted again, and new values for the $\log \sigma$ and μ_e coefficients are found, that are then used in the next iteration to obtain a new combination of the individual samples. The procedure converges typically after 3 iterations, producing a self-consistent set of peculiar velocity estimates and a FP template, which in our case is given by the relation

$$\log R_e = 1.55(\pm 0.05) \log \sigma + 0.319(\pm 0.007)(\mu_e - 19.45) - 2.916(\pm 0.0058) - \log h \tag{5.9}$$

(or equivalently $\log R_e = 1.55 \log \sigma - 0.798 \log I_e - 9.12 - \log h$), where R_e is in kiloparsec. The dispersion around this relation, measured as the rms scatter of the residuals in $\log R_e$, amounts to 0.097, which is equivalent to an uncertainty of 21% in the distance estimate of a single galaxy, or of 0.48 magnitudes in the estimate of its distance modulus.

The errors in the coefficients of equation (5.9) have been estimated using both the statistical jacknife and a bootstrap procedure, that give here almost identical results. In the statistical jacknife procedure, N sub-samples, each one composed of N-1 data-points, are extracted from the original sample of N data-points, rejecting in turn one of the data-points. In the bootstrap procedure, M sub-samples, each one composed of N data-points, are extracted from the original sample of N data-points, drawing points randomly and allowing each point to appear more than once in each sub-sample. The distribution of a certain statistical parameter (like the mean, or the standard deviation) among those N or M sub-samples is then used to estimate the uncertainty in the value of that same parameter derived from the original data-set, without having to assume an a-priori statistical distribution for the parent population of the data-set under examination (see for example Tukey 1958, and Efron 1987).

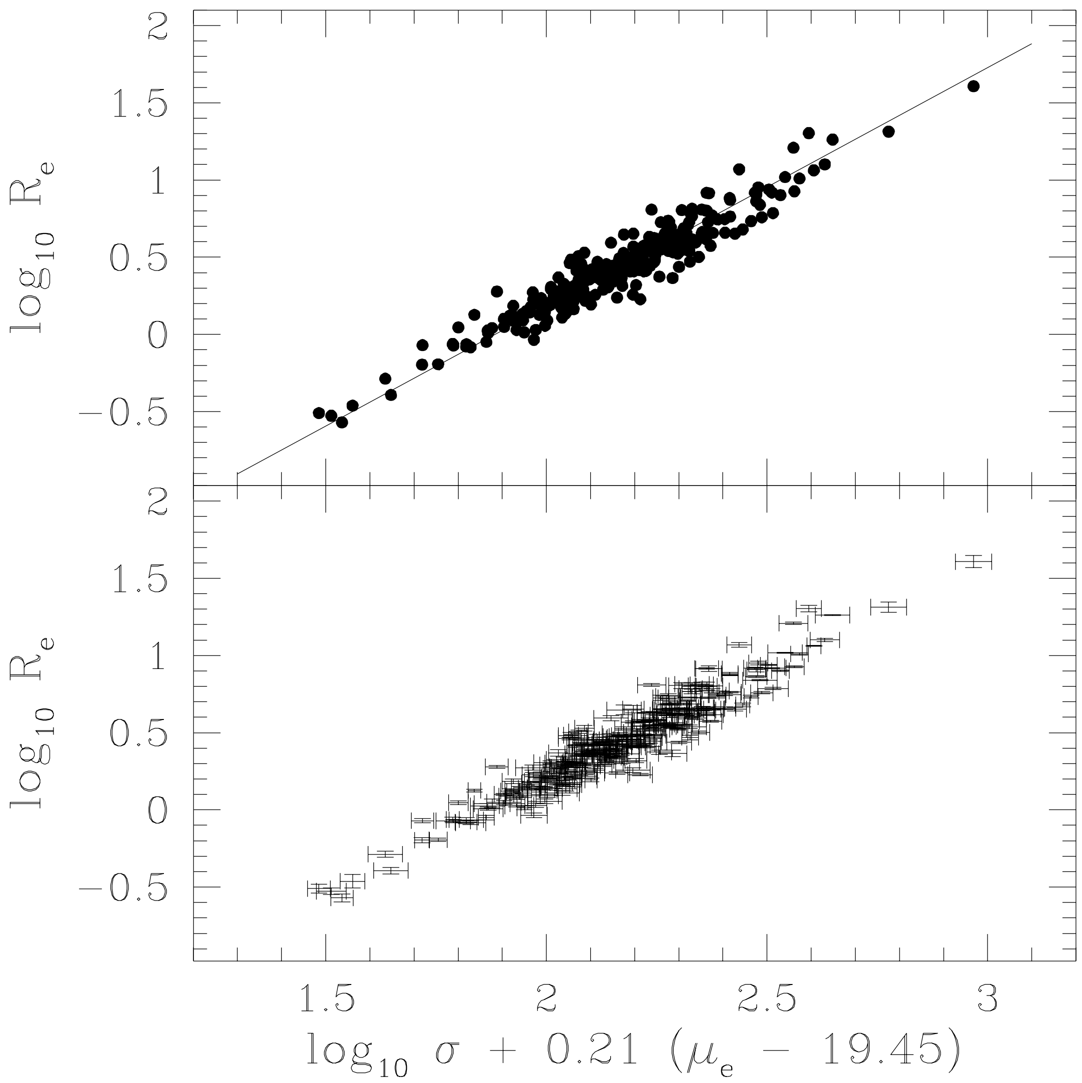

Figure 5.4 Edge-on view of the Fundamental Plane, for the combined sample of the six clusters used to derive the FP template (266 galaxies). The solid line is the projection of the FP template. Errors are plotted separately to make the figure more readable.

Figure 5.4 shows an edge-on view of the FP relation for the combined sample used to derive the FP template, composed of 266 galaxies. The solid line is the projection of the template relation (equation 5.9). A comparison with the results obtained in previous works on the FP shows that, while there is good agreement on the value of the μ_e coefficient (Djorgovski & Davis 1987 find a value of 0.36, Guzmán, Lucey & Bower 1993 a value of 0.313, and Jørgensen, Franx & Kjærgaard 1996 a value of 0.328), the $\log \sigma$ coefficient found here is significantly higher (the three works mentioned above find values of 1.39, 1.130, and 1.24). This difference appears to be due in part to the incompleteness bias corrections, not applied in the above mentioned works, that steepen the $\log R_e$ dependence on μ_e and $\log \sigma$ (the fit performed using the same six cluster sample, but the values of $\log R_e$ uncorrected for the cluster incompleteness bias gives a FP template $\log R_e = 1.45 \log \sigma + 0.310(\mu_e - 19.45) - 2.68 - \log h$), and in part to the different fitting procedures. If we remove the weighting from our fitting procedure, for example, we obtain a significantly different template relation ($\log R_e = 1.136 \log \sigma + 0.310(\mu_e - 19.45) - 1.992 - \log h$) in very good agreement with the results of Guzmán, Lucey & Bower (1993), and Jørgensen, Franx & Kjærgaard (1996). This rather large difference reflects the fact that the distributions of the measurement uncertainties in $\log \sigma$ is non-uniform, and provides also further support to the idea that a small degree of curvature might be present in the FP relation, a possibility already discussed by Djorgovski & Davis (1987) and by Jørgensen, Franx & Kjærgaard (1996), and visually appreciable in Figure 5.4.

No correlation is present between the residuals from the FP relation, measured as the residuals in $\log R_e$ with respect to the edge-on projection of the FP shown in Figure 5.4, and the most important galaxy photometric parameters, like luminosity, ellipticity, and the FP parameters themselves, as shown by the panels of Figure 5.5. A correlation is present instead with the velocity dispersion. This provides another indication that a small amount of curvature might be present in the FP relation.

A small but significant difference is present in the distribution of the residuals of the elliptical galaxies on one side, and of the S0 and S0a galaxies on the other. The histograms in Figure 5.6 show the two distributions. The difference between the means of the two distributions is 0.0286 (equivalent to a difference of 6.6% in the values of R_e). This difference is significant at a 2.2 σ level (which is equivalent to a 97.2% probability), according to a Mann-Whitney test. Similarly, a Kolmogorov-Smirnov two-samples test gives a probability of only 3.5% that the two distributions are drawn from the same population. However this result depends on the fitting procedure. A negligible difference between E and S0 galaxies of only -0.0014 (equivalent to a difference of 0.3% in the value of R_e) is present when the residuals from an unweighted-fit template are considered. A similar dependence on the parameters of the template FP relation was reported by Jørgensen, Franx & Kjærgaard (1996). This behavior is caused by the different distributions of $\log \sigma$, $\log R_e$ and μ_e between E and S0 galaxies, with the result that galaxies of the two types populate somewhat different regions of the FP. It is not clear whether these differences are intrinsic properties of the elliptical and S0 populations, or whether they are the result of some systematic misclassification of relatively distant and small galaxies. In a recent work, Jørgensen & Franx (1994) have suggested that misclassification might be the source of the apparent lack of face-on S0 galaxies in the Coma cluster. Given these considerations, we will treat here E and S0 galaxies as a homogeneous population with respect to the FP relation properties.

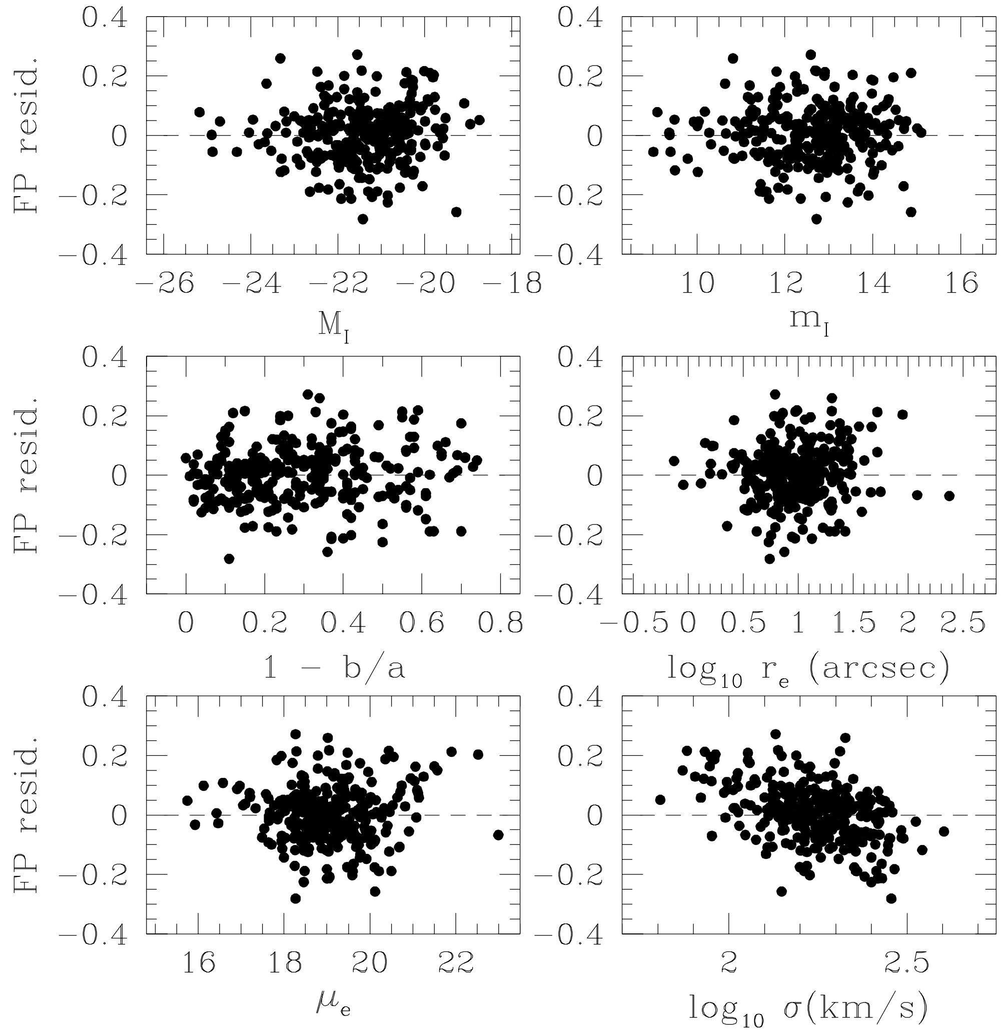

Figure 5.5 FP residuals (deviations in $\log R_e$ from the FP template) as a function of the galaxy luminosity, apparent magnitude, ellipticity, observed effective radius (in arcseconds), effective surface brightness, and velocity dispersion.

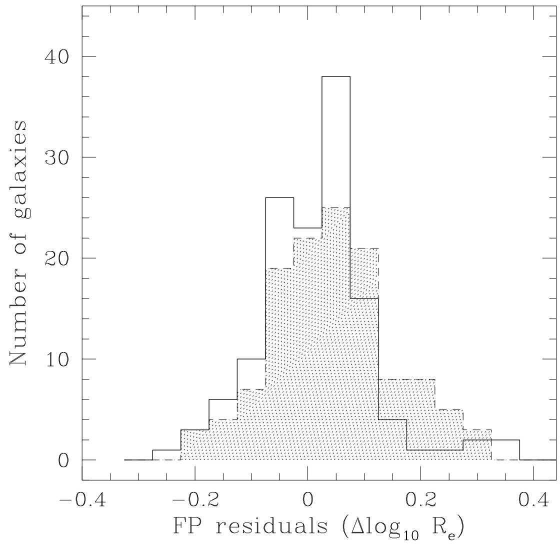

Figure 5.6 FP residuals for different morphological types. The solid line histogram represents the residual distribution for elliptical galaxies, and the shaded, dashed-line histogram the distribution for S0 and S0a galaxies.

When the whole sample of and S0 galaxies is considered, the dispersion around the FP template (equation 5.9), measured as the rms scatter of the residuals in $\log R_e$, amounts to 0.097. Measurement errors in the 3 FP parameters, once the correlation between the errors in $\log R_e$ and μ_e (section 3.6) has been taken into account, are responsible for a dispersion in $\log R_e$ of $\simeq$0.064. Subtracting this quantity from the global dispersion of 0.097, we find the intrinsic dispersion of the FP plane to be $\simeq$0.073, in good agreement with the result of Jørgensen, Franx & Kjærgaard (1996), who found an intrinsic scatter of 0.070. If E and S0 galaxies were to be considered separately, and the small difference in the mean $\log R_e$ previously discussed taken into account, then the measured dispersion around the FP template would be somewhat smaller.

5.5 The FP relation for individual clusters

The FP template described in the previous paragraph has been obtained combining together six of the individual cluster samples, under the assumption that the clusters are, on average, at rest in the CMB rest frame. The chi-square minimization then produces estimates of the relative peculiar velocities between a single cluster and the mean reference frame. These peculiar velocities are listed in Table 5.2. For the two remaining clusters (Cancer and NGC 383) that were not included in the template determination process, relative peculiar velocities were obtained again minimizing the sum of the squares of the distances from the best fitting plane (equation 5.7). In this case however the coefficients of the plane were kept fixed at the template values (equation 5.9), and only the cluster peculiar velocity was left as a free parameter in the fit. The absolute peculiar velocities of each clusters could then be obtained from the relative ones

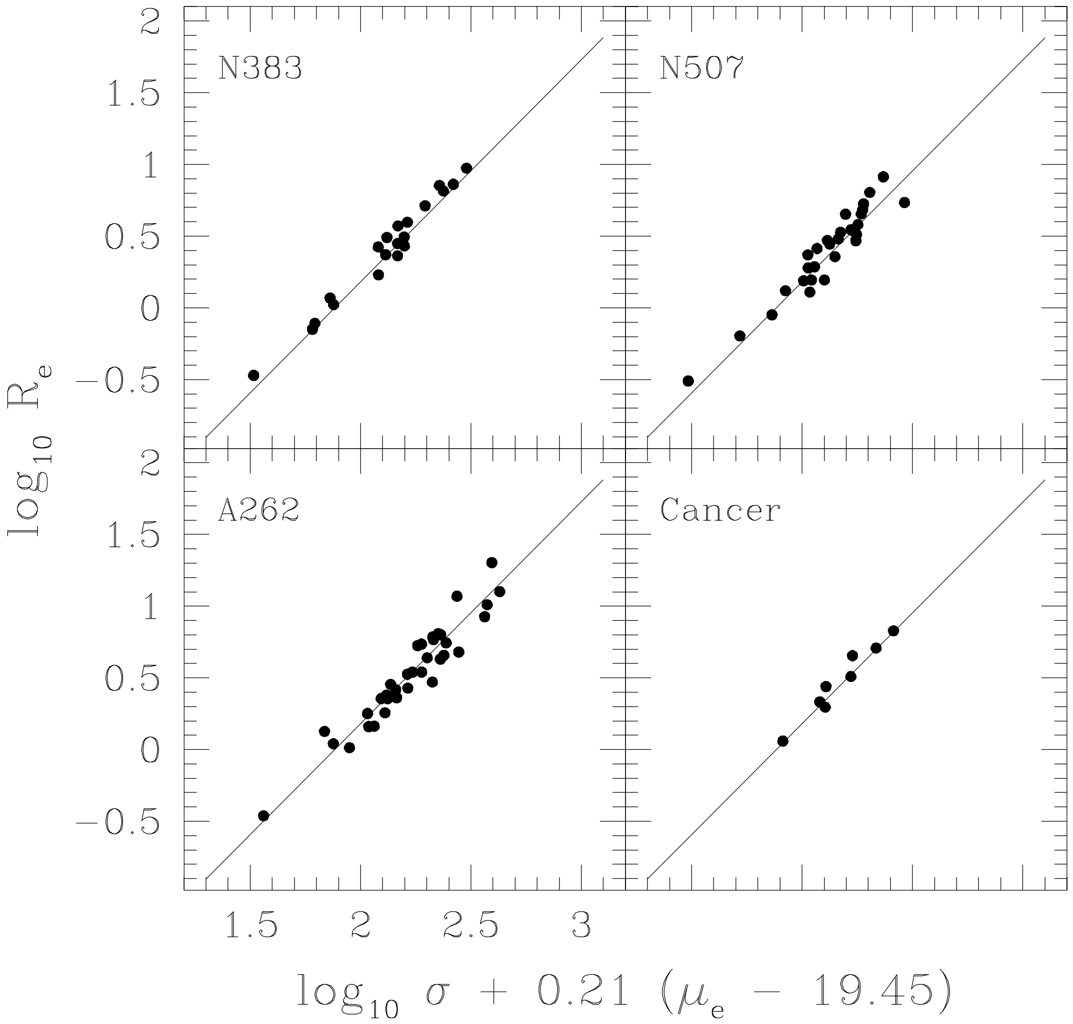

Figure 5.7 Edge-on view of the FP for the individual cluster samples. In all panels the solid line is the projection of the global FP template.

Figure 5.7 (Continued)

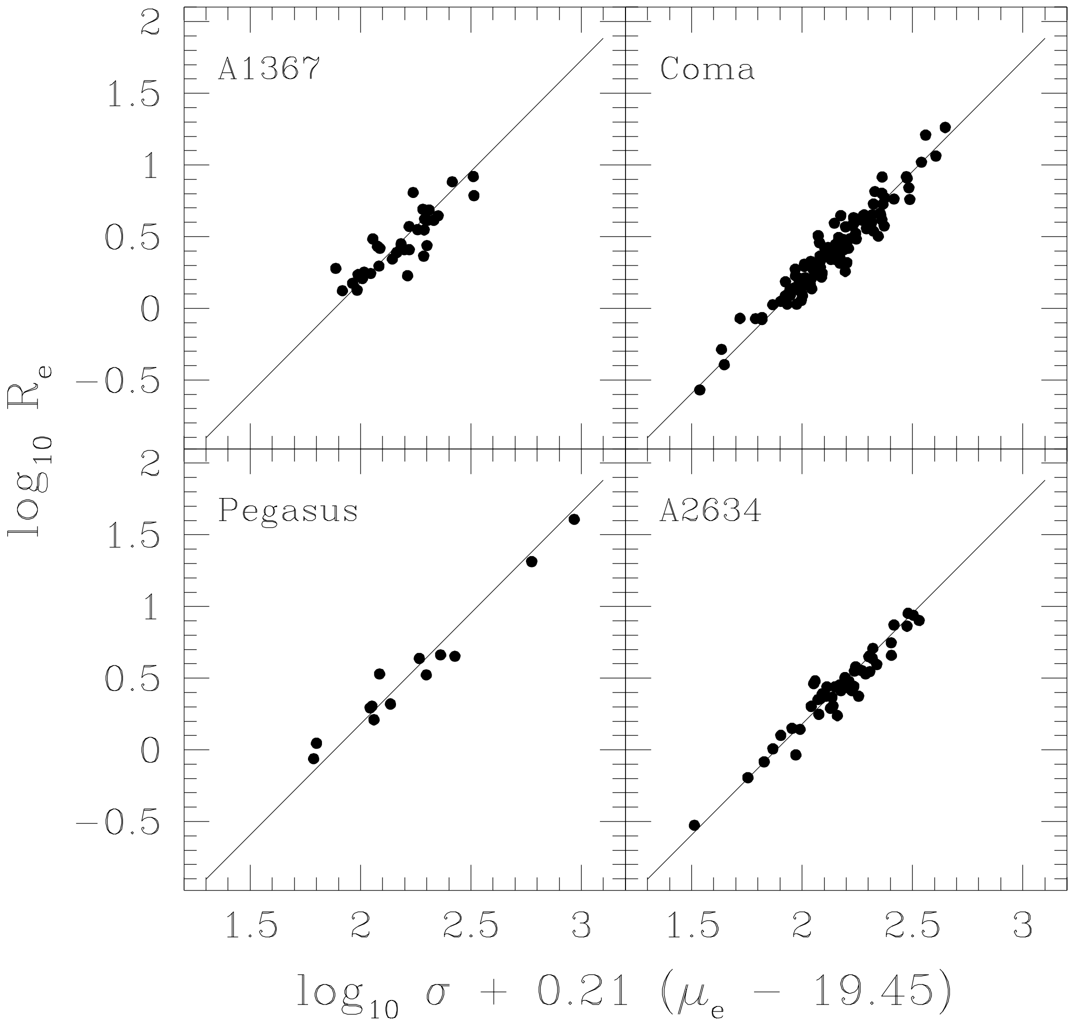

Table 5.2 Cluster peculiar velocities

Cluster	N_{gal}	$<\Delta \log R_e>$	V_{pec} (km s^{-1})
N383 gr.	20	0.0367±0.0217	429±290
N507 gr.	28	0.0206±0.0183	234±253
A262	35	-0.0099±0.0169	-105±232
Cancer	8	0.0173±0.0343	210±434
A1367	33	0.0155±0.0265	245±471
Coma	109	-0.0031±0.0093	-51±265
Pegasus	13	0.0078±0.0269	64±250
A2634	48	-0.0164±0.0140	-330±396

if a measure of the mean motion of the entire sample with respect to the CMB rest frame were available. However this is too small a sample, and one too unevenly distributed in the sky, to allow any estimate of such a mean motion.

In computing the uncertainties on the estimated peculiar velocities, an attempt has been made to take into account the uncertainty with which the six clusters used to define the FP template can approximate a reference frame at rest with respect to the CMB. From equation (5.8) one can derive that the effective radius offset $\Delta \log R_e$ is related to the peculiar velocity Δv by the relation

$$\Delta \log R_e \simeq 0.43 \frac{\Delta v}{v} \tag{5.10}$$

(if $\Delta v/v << 1$, which is appropriate for the clusters in the present sample). Here we assume that the cluster peculiar velocity distribution is characterized by a rms value of $<(\Delta v)^2>^{1/2}$, and that N randomly chosen clusters are used to map this velocity field. Then, for this sample the most probable effective radius offset from the universal FP template would be

$$\Delta \log R_e \simeq 0.43 \frac{<(\Delta v)^2>^{1/2}}{<v>} N^{-1/2} \tag{5.11}$$

Using a value $<(\Delta v)^2>^{1/2} = 293 \pm 28$ (Bahcall & Oh 1996), $<v> = 5700$ km s^{-1}, and $N = 4$ (Coma and 1367 are part of the same supercluster, and so are A262 and N507, and this reduces the number of truly independent sample points), the most likely value of effective radius offset is $\Delta \log R_e \simeq 0.011$. When this value is added in quadrature to the FP template zero-point statistical uncertainty, it gives a global uncertainty in the definition of the kinematic rest-frame of $\Delta \log R_e \simeq 0.013$. To this uncertainty we must add the offset uncertainty relative to any given cluster, and derive the uncertainty in the cluster peculiar velocity.

Together with the global FP template, individual fits have been obtained for each cluster. The parameters derived from these fits are listed in Table 5.3, and the FP relation for each individual cluster is shown in Figure 5.7. In this figure, the solid line

Table 5.3 The I band Fundamental Plane

Sample	N	$\log\sigma$ coeff.	μ_e coeff.	Zero point	dispersion
Template	266	1.548±0.050	0.319±0.007	-2.916±0.006	0.097
N383 gr.	20	1.462±0.129	0.334±0.022	-2.672±0.022	0.059
N507 gr.	28	1.500±0.189	0.328±0.028	-2.780±0.018	0.088
A262	35	1.505±0.147	0.325±0.024	-2.829±0.017	0.100
Cancer	8	1.398±0.219	0.343±0.046	-2.543±0.034	0.044
A1367	33	2.016±0.344	0.304±0.036	-3.973±0.027	0.152
Coma	109	1.548±0.095	0.323±0.010	-2.916±0.009	0.087
Pegasus	13	1.203±0.219	0.279±0.016	-2.151±0.027	0.078
A2634	48	1.688±0.141	0.307±0.013	-3.258±0.014	0.089
In ($R < 0.3R_A$)	165	1.499±0.056	0.310±0.005	-2.803±00.007	0.084
Out ($R \geq 0.3R_A$)	129	1.639±0.089	0.333±0.013	-3.114±0.010	0.110

is again the global FP template (equation 5.9). Note that in this figure the values of $\log R_e$ have not been corrected for the effect of the peculiar velocities listed in Table 5.2. Looking at Figure 5.7, and at Table 5.3, it is clear that there are no significant differences among the individual cluster samples.

A simple test for the presence of environmental effects can be performed analyzing the distribution of FP parameters as a function of galaxy position within the cluster. Figure 5.8 shows the residuals from the FP template (equation 5.9) for the entire combined sample, where the angular distances of individual galaxies from their relative cluster center have been normalized in terms of the Abell radius of the cluster. Similarly, separate fits to the samples composed of the objects within 0.3 Abell radii from their cluster center, and of the objects outside those radii, produce results that are not significantly different. The results of those fits are listed in Table 5.3, together with the individual cluster fits, and the six-cluster template fit. Another way to look for environmental effects is to analyze the possible presence of correlations between the FP parameters and cluster properties like the velocity dispersion, and the X-ray luminosity and temperature. All these quantities provide a measure of the richness of the cluster, and of its degree of dynamical evolution, and therefore should provide a measure of the strength of the environmental effects that might bias the FP relation. As shown by the panels of Figure 5.9, no significant correlation is present, for a sample that spans two orders of magnitude in X-ray luminosity, and approximately a factor of three in velocity dispersion. These simple tests already show that no strong environmental effect, of the kind previously reported by Djorgovski, de Carvalho & Han (1988), is present in the FP relation.

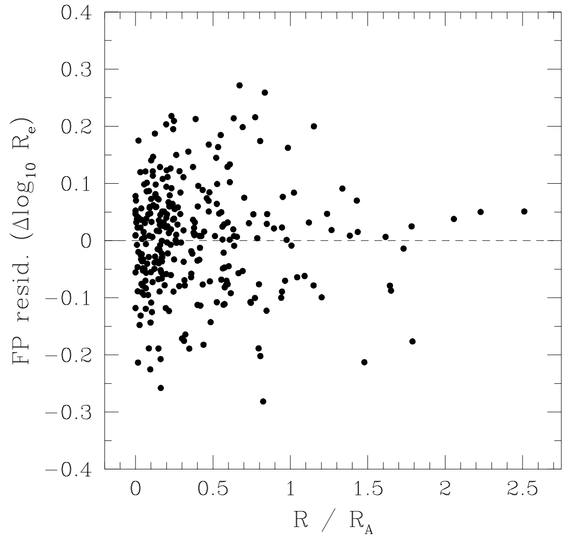

Figure 5.8 FP residuals as a function of the galaxy angular distance from the relative cluster center. Angular distances in different clusters are normalized to the Abell radius of each cluster.

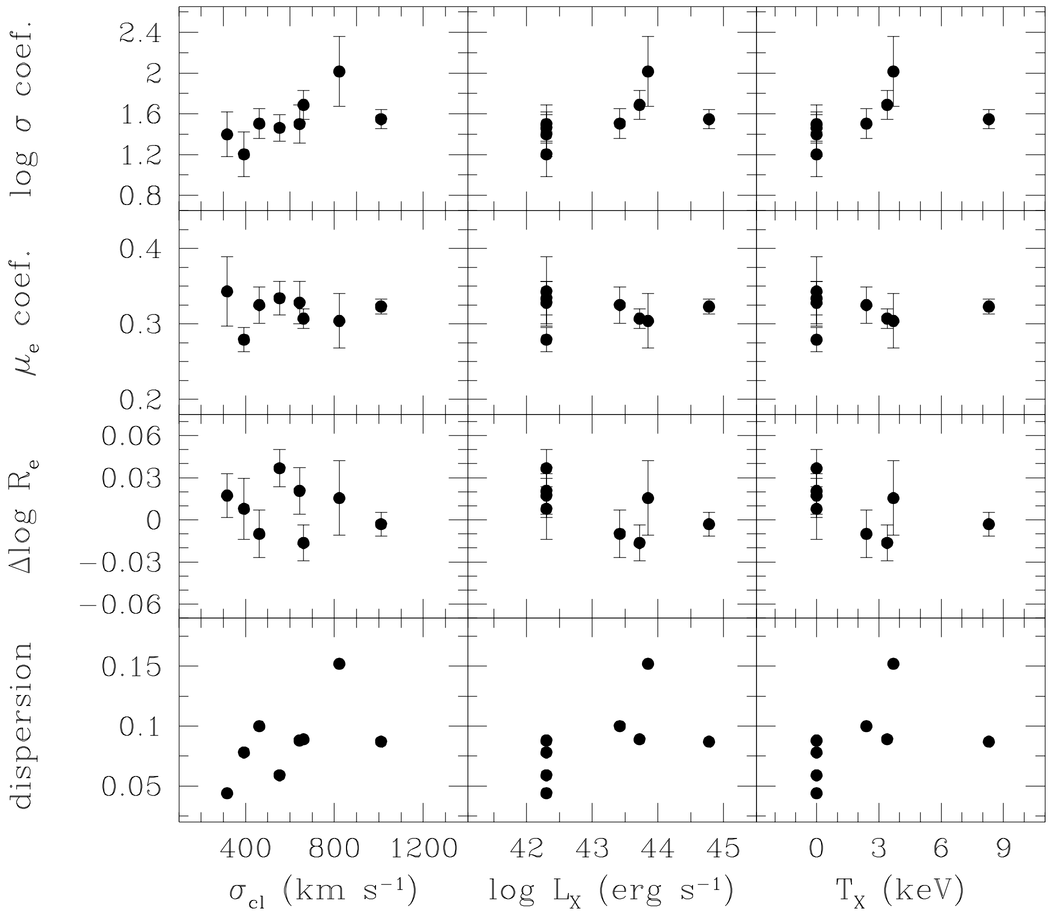

Figure 5.9 The distribution of the FP parameters as a function of the cluster velocity dispersion, X-ray luminosity in the 2-10 keV band, and X-ray temperature.